Neoadjuvant FOLFIRINOX Therapy Is Associated with Increased Effector T Cells and Reduced Suppressor Cells in Patients with Pancreatic Cancer

Hui Peng[1], C. Alston James[1], Darren R. Cullinan[1], Graham D. Hogg[2], Jacqueline L. Mudd[1], Chong Zuo[2], Rony Takchi[1], Katharine E. Caldwell[1], Jingxia Liu[1], David G. DeNardo[2,3], Ryan C. Fields[1,3], William E. Gillanders[1,3], S. Peter Goedegebuure[1,3], and William G. Hawkins[1,3]

ABSTRACT

Purpose: FOLFIRINOX has demonstrated promising results for patients with pancreatic ductal adenocarcinoma (PDAC). Chemotherapy-induced immunogenic cell death can prime antitumor immune responses. We therefore performed high-dimensional profiling of immune cell subsets in peripheral blood to evaluate the impact of FOLFIRINOX on the immune system.

Experimental Design: Peripheral blood mononuclear cells (PBMC) were obtained from treatment-naïve ($n = 20$) and FOLFIRINOX-treated patients ($n = 19$) with primary PDAC tumors at the time of resection. PBMCs were characterized by 36 markers using mass cytometry by time of flight (CyTOF).

Results: Compared with treatment-naïve patients, FOLFIRINOX-treated patients showed distinct immune profiles, including significantly decreased inflammatory monocytes and regulatory T cells (Treg), increased Th1 cells, and decreased Th2 cells. Notably, both monocytes and Treg expressed high levels of immune suppression-associated CD39, and the total $CD39^+$ cell population was significantly lower in FOLFIRINOX-treated patients compared with untreated patients. Cellular alterations observed in responders to FOLFIRINOX included a significantly decreased frequency of Treg, an increased frequency of total CD8 T cells, and an increased frequency of $CD27^-Tbet^+$ effector/effector memory subsets of CD4 and CD8 T cells.

Conclusions: Our study reveals that neoadjuvant chemotherapy with FOLFIRINOX enhances effector T cells and downregulates suppressor cells. These data indicate that FOLFIRINOX neoadjuvant therapy may improve immune therapy and clinical outcome in patients with PDAC.

Introduction

Pancreatic cancer is one of the deadliest cancers and is expected to become the second-leading cause of cancer-related death by 2030 (1–3). Currently, the 5-year survival rate for all stages of pancreatic cancer is approximately 9% (4). Systemic adjuvant therapy with FOLFIRINOX, comprised of 5-fluorouracil, leucovorin, irinotecan, and oxaliplatin, demonstrates the most promising results (2, 4–6). However, as evidenced by the poor overall survival rate, there is an acute need to improve therapies for pancreatic ductal adenocarcinoma (PDAC). Increasing evidence suggests that neoadjuvant chemotherapy has a beneficial effect on overall survival in resectable PDAC in comparison with upfront resection (2, 7). Unfortunately, not all patients respond to neoadjuvant FOLFIRINOX chemotherapy, indicating the existence of patient or tumor factors which must be further explored to improve this therapeutic strategy.

Conventional chemotherapy can not only induce cancer cell death by cytostatic and direct cytotoxic effects, but can also exert immunomodulatory effects (8). Some chemotherapeutic agents have the capacity to trigger immunogenic cell death (8, 9). Immunogenic cell death is associated with a particular type of apoptosis in which dying and dead cells act as antigens that induce immune responses. Oxaliplatin, a known immunogenic cell death inducer, has been found to release ATP from tumor cells, boosting their immunogenicity (10, 11). On the basis of these findings, we hypothesized that FOLFIRINOX impacts immune cell composition and activity in patients with PDAC and the status of a patient's immune system may determine therapeutic efficacy.

Prior studies of immune checkpoint monotherapy have failed to demonstrate meaningful clinical responses in patients with PDAC (12). In PDAC, the low proportion of tumor-infiltrating lymphocytes has been associated with both low mutational burden and frequency of neoantigens (13, 14). In addition, PDAC is characterized by a highly immunosuppressive tumor microenvironment that can impede both the activation and effector function of tumor reactive CTLs (14) by diminished antigen presentation through dendritic cells (15, 16), the presence of protumor T-cell subsets (Treg and Th2 cells; refs. 17, 18), and immunosuppressive cytokines (19, 20). This immunosuppressive microenvironment may explain why immune checkpoint blockade monotherapy has no clinical efficacy in PDAC, despite its effectiveness in various other cancer types (21).

The success of chemotherapy is often impacted by immune cell subsets in the tumor microenvironment (9, 22), highlighting the potential of combining neoadjuvant chemotherapy and immunotherapy. However, little is known about the impact of neoadjuvant FOLFIRINOX on the immune system in patients with PDAC. A comprehensive study using IHC and immunofluorescence in PDAC tissues identified a shift toward antitumor immunity after neoadjuvant

[1]Department of Surgery, Washington University School of Medicine, St. Louis, Missouri. [2]Department of Medicine, Washington University School of Medicine, St. Louis, Misoouri. [3]Siteman Cancer Center, Washington University School of Medicine, St. Louis, Missouri.

Note: Supplementary data for this article are available at Clinical Cancer Research Online (http://clincancerres.aacrjournals.org/).

Corresponding Author: William G. Hawkins, Department of Surgery, Washington University in St. Louis, 660 South Euclid Avenue, St. Louis, MO 63110. Phone: 314-362-7046; E-mail: hawkinsw@wustl.edu

Clin Cancer Res 2021;27:6761–71

doi: 10.1158/1078-0432.CCR-21-0998

Translational Relevance

FOLFIRINOX has demonstrated promising clinical results for patients with pancreatic ductal adenocarcinoma (PDAC). While the immunogenicity of certain chemotherapeutics has been demonstrated, little is known about the impact of neoadjuvant FOLFIRINOX chemotherapy on the immune system in patients with PDAC. Here we performed immune phenotype analysis by CyTOF in peripheral blood of untreated patients and FOLFIRINOX-treated patients in the neoadjuvant setting. Distinct immune profiles were observed in FOLFIRINOX-treated patients, including increased Th1 cells and decreased classical monocytes, Th2 cells, and suppressor subsets. Cellular alterations observed in clinical responders to FOLFIRINOX included an increased CD8 T-cell frequency and increased $CD27^{-}Tbet^{+}$ phenotypic fractions in CD4 and CD8 T cells. Our study suggests that neoadjuvant chemotherapy with FOLFIRINOX may enhance functional T cells and downregulate suppressor cells. Taken together, these findings indicate that neoadjuvant FOLFIRINOX may improve immune therapy and clinical outcome in patients with PDAC.

chemotherapy (22). As induction of systemic immunity is likely required for long-term protection post-surgery, we studied here the immunologic impact of neoadjuvant FOLFIRINOX through analysis of peripheral blood samples using mass cytometry by time of flight (CyTOF). We prioritized identification of immune subsets, as well as markers of activation and cytotoxicity. Our study identified substantial differences in peripheral blood mononuclear cells (PBMC) from FOLFIRINOX-treated and untreated patients. Furthermore, we characterized specific immune profiles present in responders and nonresponders to FOLFIRINOX neoadjuvant therapy. These studies indicate that FOLFIRINOX neoadjuvant therapy may improve immune therapy and clinical outcome in patients with PDAC.

Materials and Methods

Patient samples

We identified two groups of patients with pancreatic cancer samples collected from May 2014 to May 2019 using the tissue bank funded by the Washington University SPORE in Pancreas Cancer in the Department of Surgery. Patient characteristics are summarized in Supplementary Table S1. These groups include patients who had upfront surgical resection without neoadjuvant chemotherapy ($n = 20$) and patients who had surgical resection after neoadjuvant chemotherapy with FOLFIRINOX ($n = 19$). The FOLFIRINOX regimen consisted of oxaliplatin, leucovorin, irinotecan, and fluorouracil. Patients treated with at least three cycles of FOLFIRINOX were included in this analysis (Supplementary Table S2). Clinical responses to FOLFIRINOX treatment such as complete response, partial response, stable disease, and progressive disease were determined on the basis of RECIST 1.1 (23). Tumor size was defined as the maximal diameter of the lesion as reported on cross-sectional imaging. In these studies, we defined response to FOLFIRINOX as a reduction in tumor size by more than 30%. All responses were determined by a radiologist. Nine of the 19 patients treated with FOLFIRINOX were considered responders with a reduction in tumor volume ranging from 32% to 65%. Ten of the 19 patients were considered nonresponders with less than 30% reduction in tumor volume. PBMC were obtained from untreated and FOLFIRINOX-treated patients with primary PDAC tumors at the time of resection. The study was conducted in accordance with U.S. Common Rule and was approved by the Institutional Review Board at Washington University School of Medicine (St. Louis, MO). All patients provided written informed consent for study participation and the use of biomaterial for translational research. All blood samples were collected pre-operation. PBMC were isolated from freshly drawn heparin anticoagulated blood by density gradient separation with Ficoll-Paque PLUS (GE Healthcare Bio-Sciences), then cryopreserved in FBS containing 10% DMSO (Sigma-Aldrich) and stored in liquid nitrogen.

Intracellular cytokine analysis and flow cytometry

Cryopreserved PBMC were thawed in a 37°C water bath and washed in prewarmed cell culture medium (RPMI1640, 10% FCS, 1× L-glutamine, and 1×penicillin/streptomycin supplemented with 1:10,000 benzonase (Sigma-Aldrich). Cells were then rested in complete medium (RPMI1640, 1× L-glutamine, and 1×penicillin/streptomycin supplemented with 10% FBS) for 1 hour at 37°C before stimulation. Cells were stimulated for 4 hours with 50 ng/mL phorbol-12-myristate-13-acetate (PMA; Sigma) and 500 ng/mL ionomycin (Sigma) in the presence of Golgiplug (BD). Cells were then washed with PBS and live/dead stained with V450 (Invitrogen) for 15 minutes at room temperature. Cells were incubated with anti-CD4 (RRID: AB_2616809) and anti-CD8 (RRID: AB_2044009) antibodies for 30 minutes at 4°C in the dark. After washing with FACS buffer, samples were then fixed and permeabilized to perform intracellular staining. Cells were incubated with an intracellular antibody cocktail [anti-IFNγ (RRID: AB_961351) and anti-TNFα (RRID: AB_315261)] for 45 minutes at 4°C in the dark. Cells were acquired by flow cytometry (BD FACScan) and data were analyzed with Flowjo software (RRID: SCR_008520).

Mass cytometry

Monoclonal anti–human antibodies (Supplementary Table S3) were purchased from Fluidigm. Antibodies for RORγt (RRID: AB_2561797), GITR(RRID:AB_314885), and CTLA-4 (RRID: AB_2566610) were purchased from BioLegend and conjugated in-house to heavy-metal isotopes from commercial suppliers using the Maxpar X8 chelating polymer kit (Fluidigm) according to the manufacturer's instructions.

Cryopreserved PBMC were thawed in a 37°C water bath and washed in 9 mL of prewarmed cell culture medium. Cells were then rested in complete medium for 1 hour at 37°C before staining. PBMC (3×10^6) were first stained with 5 mmol/L cisplatin (Sigma) for 3 minutes on ice. After blocking with 50 μg/mL of human IgG (BD Biosciences) for 5 minutes, cells were stained with a master mix of titrated amounts of metal-labeled antibodies (Supplementary Table S3) at 4°C for 45 minutes. Surface-stained cells were permeabilized and fixed using FOXP3/Transcription Factor Staining Buffer (Thermo Fisher Scientific) for 45 minutes on ice. After washing in permeabilization buffer (Thermo Fisher Scientific), cells were then incubated for intracellular staining with a titrated panel of antibodies in permeabilization buffer for 45 minutes on ice. After washing in CytoPBS, cells were stained with 62.5 nmol/L Iridium nucleic acid intercalator (Fluidigm) diluted in 2% paraformaldehyde (Electron Microscopy Sciences) in PBS overnight at 4°C. Finally, the cells were washed once with PBS, once with MilliQ water, and then diluted in water containing 10% EQ Calibration Beads (Fluidigm) before acquisition on a CyTOF2 mass cytometer (Fluidigm).

Data acquisition on CyTOF2 mass cytometer and data preprocessing

Samples were acquired on a CyTOF2 mass cytometer (DVS Sciences/Fluidigm). FCS files were normalized by adding five-element beads (Fluidigm) to the sample immediately before acquisition and using the Matlab-based normalization software as described previously (24). Next, individual samples were manually gated using Cytobank (RRID: SCR_014043) to exclude normalization beads, cell debris, and dead cells for the identification of $CD45^+Cisplatin^-$ events, which were exported as new FCS files (Supplementary Fig. S1). The newly created FCS files were then batch normalized by the date of acquisition using the R Cydar package Normalize Batch function (mode = "range") to compute a quantile function from the pooled distribution of the input expression data (25). In brief, batch expression was scaled between the upper and lower bounds of the pooled reference distribution, with zero values fixed at zero. Normalized files were then uploaded into Cytobank and we then removed doublets by removing CD3/CD19 and CD3/CD14 double positive cells. Immune profiles were analyzed through the Cytobank cloud-based platform for two-dimensional (2D) visualization using viSNE and identification of immune cell subsets was performed using hierarchical clustering approaches in FlowSOM. To assess the reproducibility of the CyTOF analysis, we performed staining and analysis on PBMC from the same patients in three independent experiments. Data analysis showed that the average % coefficient of variation for the cell populations was less than 10% (Supplementary Fig. S2).

Automated population identification in high-dimensional data analysis

viSNE is an automated dimensionality reduction algorithm which allows one to map high-dimensional cytometry data onto two dimensions and conserve the high-dimensional structure of the data. To run viSNE in CytoBank, we uploaded the normalized FCS files of all patients to CytoBank. Subsequent analyses were performed on live $CD45^+$ cells. 28 markers: CD11b, CD3, CD4, CD8, CD19, CD56, CD14, CD16, CD39, CD45RA, CCR7, CD27, CD39, TIGIT, PD1, CD25, CD38, CXCR3, CCR6, CCR4, GATA3, Tbet, FOXP3, Ki67, IgD, BTLA, CXCR4, and Granzyme B (GzmB), were used to build the map. Markers with low expression were excluded as they would not contribute to the structure of the map. Equal sampling of 12,000 cells per file was performed. Once maps were generated, the expression level and distribution of each marker of interest was visualized by color.

To better dissect T-cell heterogeneity, separate viSNE plots were generated for all samples on the following manually gated populations: (i) $CD45^+CD3^+CD56^-CD8^+$ and (ii) $CD45^+CD3^+CD56^-CD4^+$. For visualization with viSNE, 5,333 cells/sample and 1,870 cells/sample were used for $CD4^+$ and $CD8^+$ T cells, respectively. Sixteen markers: CD45RA, CCR7, CD27, CD39, TIGIT, PD1, CD25, CXCR3, CCR4, GATA3, Tbet, FOXP3, Ki67, GzmB, CCR6, and Perforin were used to build the map for $CD4^+$ T cells. Fifteen markers: CD45RA, CCR7, CD27, CD39, TIGIT, PD1, CD25, CXCR3, CCR4, GATA3, Tbet, Ki67, GzmB, CXCR4, and Perforin were used to build the map for $CD8^+$ T cells.

For $CD39^+$ cells, we manually gated on $CD39^+CD45^+$ cells and then viSNE was performed on the expression of 20 markers: CD11b, CD14, CD16, CD19, CCR6, CD3, CD4, CD8, CD56, CD27, TIGIT, CD45RA, CCR4, CCR7, FOXP3, PD1, PDL1, ICOS, CD25, and CD24.

FlowSOM

FlowSOM is an algorithm that speeds time to analysis and quality of clustering with self-organizing maps (SOM) that can reveal how all markers are behaving on all cells (26). Unsupervised clustering was performed on the expression values of lineage markers using the FlowSOM algorithm in Cytobank. For all analyses, we selected equal cell numbers for each sample. Channel (marker) selection was variable depending on cell populations to be clustered.

For $CD45^+$ cells, we included all samples (12,000 cells/sample) and the following markers were used for clustering: CCR4, CCR7, CD14, CD16, CD19, CD27, CD3, CD39, TIGIT, CD4, CD45RA, CD8, CXCR3, FOXP3, GATA3, ICOS, CD25, and CD56. Clusters with <0.6% of the analyzed cells were excluded. Heatmaps were used to display median expression.

For $CD4^+$T cells, 5,333 cells/sample were clustered and 16 markers: CD45RA, CCR7, CD27, CD39, TIGIT, PD1, CD25, CXCR3, CCR4, GATA3, Tbet, FOXP3, Ki67, GzmB, CCR6, and Perforin were used to build the viSNE map for CD4 T cells. After viSNE plots were generated, we defined Treg and non-Treg subsets based on expression of CD25 and FOXP3. We then performed FlowSOM for non-Treg subsets to segregate cell populations based on expression of CD45RA, CXCR3, CCR4, and CCR6. From this, we defined Th1 ($CXCR3^+CCR6^-$), Th17 ($CXCR3^-CCR6^+$), Th17.1 ($CXCR3^+CCR6^+$), and Th2 ($CXCR3^-CCR6^-CCR4^+$) populations.

Statistical analysis

GraphPad Prism7 (RRID: SCR_002798) was used for all statistical analyses. Differences between groups or experimental conditions were determined using a two-tailed Mann–Whitney Wilcoxon test. Correlations were analyzed using Pearson correlation. Survival probabilities were estimated using the Kaplan–Meier method and survival differences were compared using the log-rank test. Two-sided P values <0.05 were considered as statistically significant for all the analysis.

Results

Neoadjuvant chemotherapy with FOLFIRINOX was not associated with improved survival from the time of resection

Chemotherapy with FOLFIRINOX has shown clinical benefit to patients treated in the adjuvant setting (5) or for patients with metastatic disease (27). However, treatment in the neoadjuvant setting has shown mixed responses (28–30). To assess the clinical relevance of neoadjuvant FOLFIRINOX in our cohort of patients with patients with PDAC, we analyzed Kaplan–Meier survival curves in FOLFIRINOX-treated (FFX, $n = 19$) versus treatment-naïve patients (NT, $n = 20$). FOLFIRINOX treatment was not associated with improved survival from the time of resection. Not surprisingly, patients who clinically responded to FOLFIRINOX treatment (FFX-R, $n = 9$) exhibited improved disease-free survival as well as overall survival when compared with nonresponders (FFX-NR, $n = 10$; **Fig. 1A** and **B**).

FOLFIRINOX enhances T cell–mediated cytokine production

Chemotherapy using 5-fluorouracil and oxaliplatin has been demonstrated to improve antitumor T-cell functions (9). We therefore investigated whether neoadjuvant chemotherapy with FOLFIRINOX affects the immune phenotype in patients with PDAC. We first assessed cytokine production in treatment-naïve (NT, $n = 6$) and FOLFIRINOX-treated patients (FFX, $n = 10$) following PMA/ionomycin stimulation of PBMC by multicolor flow cytometry. The results show that treated patients have more $IFN\gamma^+TNF\alpha^+CD8^+$T cells than untreated patients (**Fig. 2**; Supplementary Fig. S3), suggesting FOLFIRINOX treatment enhances activation of CD8 T cells.

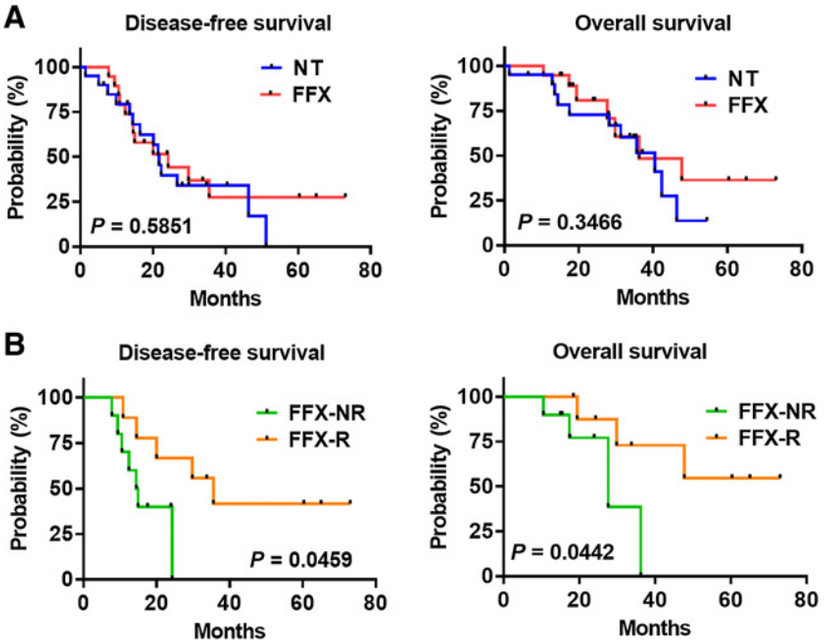

Figure 1.
Response to FOLFIRINOX neoadjuvant therapy correlates with better outcome in pancreatic cancer. **A,** Disease-free survival and overall survival for treatment-naïve patients (NT, $n = 20$) and patients treated with FOLFIRINOX neoadjuvant therapy (FFX, $n = 19$). **B,** Disease-free survival and overall survival for responders (FFX-R, $n = 9$) and nonresponders (FFX-NR, $n = 10$) to FOLFIRINOX neoadjuvant therapy.

Unsupervised analysis reveals distinct immune cell subsets in PBMC from patients with PDAC

To further investigate the immune alterations caused by FOLFIRINOX, we performed high-dimensional analysis on PBMC samples obtained immediately prior to surgery isolated from patients with resectable PDAC that underwent upfront resection from both treatment-naïve and FOLFIRINOX-treated patients. We employed a staining panel containing 36 leukocyte markers to identify all major immune cell populations and cover all stages of T-cell differentiation and activation markers (Supplementary Table S3).

To perform a qualitative analysis of the PBMC immunophenotyping data, we first applied viSNE dimensional reduction on the immune cell abundance profiles from all patients with PDAC. This analysis demonstrated the heterogeneity of major immune cell lineages across immune profiles, which can be further defined using t-SNE maps colored by marker intensities (**Fig. 3**; Supplementary Fig. S4). Next, we sought to identify which cell population best described the differences between treatment-naïve (NT, $n = 20$) and FOLFIRINOX-treated (FFX, $n = 19$) patients. Unsupervised cluster analysis revealed 15 populations, which were identified through the median expression of lineage markers as shown in **Fig. 3B** and **C**; Supplementary Table S4. The frequency of each of the clusters varied by patient (**Fig. 3D**).

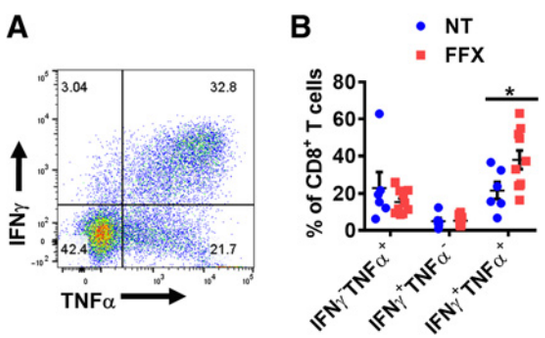

Figure 2.
FOLFIRINOX neoadjuvant therapy is associated with CD8 T-cell activation. **A,** *In vitro* analysis of IFNγ- and TNFα-producing $CD8^+$ T cells following PMA/ionomycin stimulation in PBMC from treatment-naïve patients with PDAC (NT, $n = 6$) and patients treated with FOLFIRINOX (FFX, $n = 10$). **B,** The percentage of cytokine producing cells is shown. Graphical data represent the mean ± SEM and were analyzed by Mann–Whitney Wilcoxon test. *, $P < 0.05$.

Immune profiles differ between treatment-naïve and FOLFIRINOX-treated PDAC patients

We subsequently examined differences in frequencies of the identified clusters between the FOLFIRINOX and treatment-naïve groups. In the FOLFIRINOX treatment group, the frequencies of both $CD14^+CD16^-$ classical monocytes and $CD4^+$ Treg as a percentage of all leukocytes were significantly lower than in the untreated group (**Fig. 4A**). The frequencies of $CD4^+CD8^+$double positive T cells (DPT) were significantly higher in FOLFIRINOX treatment than in the untreated patients. All other subsets were not significantly different in these two groups (**Fig. 4A**).

To better characterize the phenotype of $CD4^+$ T cells, we gated on $CD3^+CD4^+CD56^-$ cells and performed a viSNE analysis. Treg subpopulations were clustered and identified by high expression of CD25 and FOXP3 (**Fig. 4B**). $CD25^+FOXP3^+$ Treg also express CD39 (**Fig. 4B**). CD39 can be expressed on the surface of cancer cells and regulatory immune cells. CD39 is an ectonucleotidase which can convert ATP into adenosine (31) suppressing T-cell function (32). We found that the patients treated with FOLFIRINOX showed a significantly lower frequency of Treg compared with treatment-naïve patients (**Fig. 4C**).

The expression of chemokine receptor CCR4, CXCR3, and CCR6 can be used for identification of Th2 ($CCR4^+CXCR3^-CCR6^-$), Th1 ($CXCR3^+CCR6^-$), Th17 ($CXCR3^-CCR6^+$), and Th17.1 ($CXCR3^+CCR6^+$) CD4 T-cell subsets (33–35). To determine whether there were differences in CD4 T-cell subsets between patient groups, we

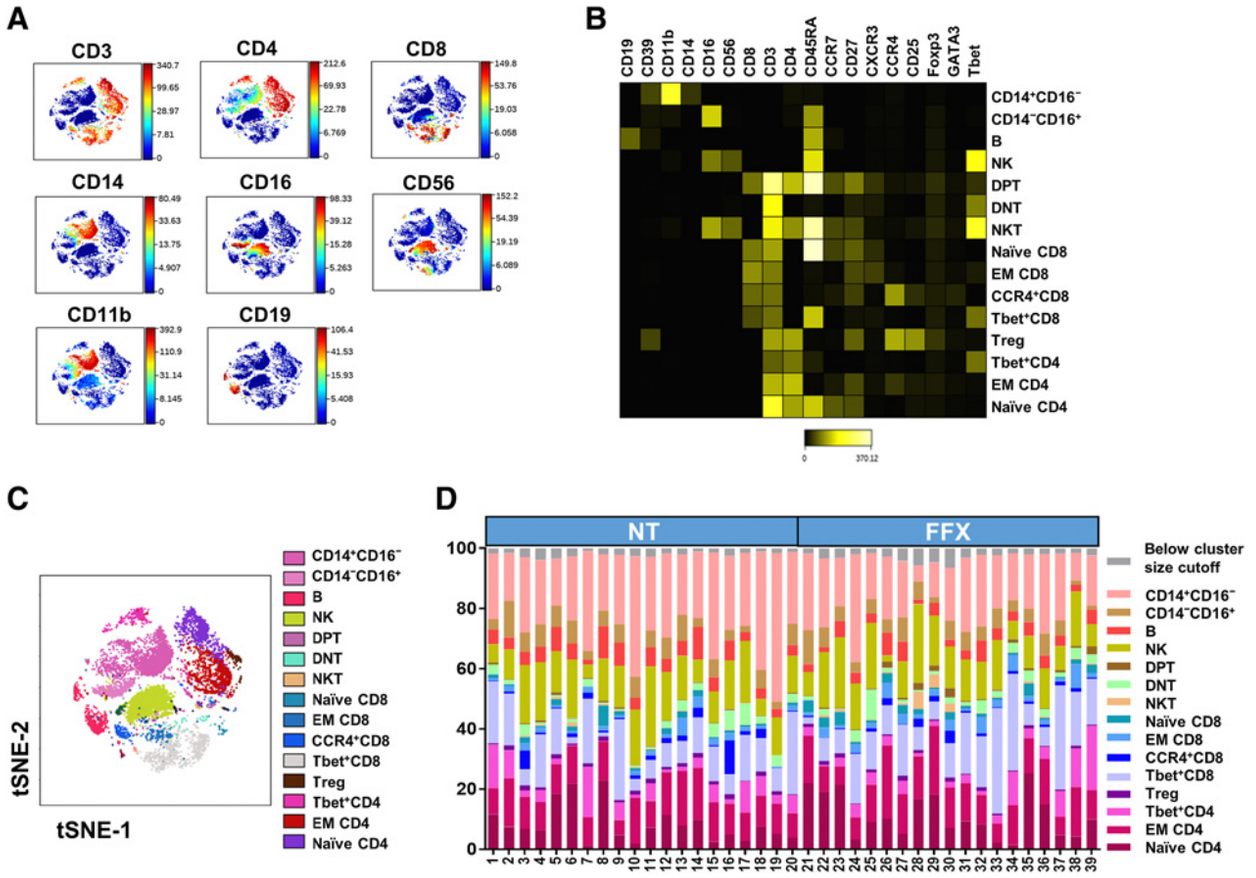

Figure 3.

Unsupervised analysis of CyTOF data reveals distinct immune cell clusters in PBMC from FOLFIRINOX-treated patients with PDAC. **A,** Two-dimensional cellular illustration of CD3, CD4, CD8, CD14, CD16, CD11b, CD56, and CD19 in PBMC by viSNE maps. **B,** Unsupervised clustering analysis with FlowSOM revealed 15 distinct cell clusters. A heatmap summary of the expression values of 18 lineage markers was used to distinguish cell subsets. **C,** The t-SNE algorithm was used to depict the major immune populations in PBMC. **D,** Stacked bar graph representing all cell clusters identified in each patient, including treatment-naïve patients (NT, $n = 20$) and FOLFIRINOX-treated patients (FFX, $n = 19$). Clusters comprising <0.6% of the analyzed cells were excluded from all other analyses and are represented here as "below cluster size cutoff."

ran FlowSOM analysis on non-Treg $CD4^+$ T cells based on CD45RA, CXCR3, CCR6, and CCR4. Cells were subdivided into eight subsets, including: $CXCR3^+CCR4^-$ ($CCR4^-$ Th1), $CXCR3^+CCR4^{low}$ ($CCR4^{low}$ Th1), $CXCR3^+CCR4^+$, $CCR4^+CCR6^-CXCR3^-$ (Th2), $CCR4^+CCR6^+$ ($CCR4^+$ Th17), $CXCR3^+CCR6^+$ (Th17.1), $CCR4^-CCR6^+$ ($CCR4^-$ Th17) and $CD45RA^+$ cells (**Fig. 4D** and **E**; Supplementary Fig. S5). We found that all of the Th1, Th2, Th17, and Th17.1 cells were $CD45RA^-$ cells. Then we compared the frequencies of resultant T-cell subclusters of $CD45RA^-CD4^+$ T cells between treatment and nontreatment groups. Patients treated with FOLFIRINOX showed a significantly higher frequency of Th1, $CCR4^-$ Th17, and Th17.1 cells compared with treatment-naïve patients (**Fig. 4F**). The FOLFIRINOX-treated patients showed significantly lower Th2 proportions compared with treatment-naïve patients (**Fig. 4F**).

FOLFIRINOX patients have fewer CD39-expressing cells in the periphery than treatment-naïve patients

As shown in **Fig. 4A**, a significantly higher frequency of $CD14^+CD16^-$ monocytes was observed in treatment-naïve patients compared with the FOLFIRINOX group. Interestingly, we found monocytes expressed high levels of CD39 (**Fig. 5A** and **B**). CD39 was recently reported to be a new immune checkpoint target for cancer immunotherapy (36). To analyze CD39-expressing PBMC, we performed gating on total $CD39^+CD45^+$ cells in each patient group (**Fig. 5A**) and observed that the proportion of $CD39^+CD45^+$ cells was significantly lower in the FOLFIRINOX-treated patients compared with untreated patients but was similar between responders and nonresponders to FOLFIRINOX (**Fig. 5C**; Supplementary Fig. S6A). In treatment-naïve patients, the frequency of $CD39^+CD45^+$ cells negatively correlated with CD8 T cells (**Fig. 5D**), suggesting $CD39^+CD45^+$ cells might suppress CD8 T cells. In fact, *in vitro* studies confirmed CD39-mediated inhibition of T-cell proliferation (Supplementary Fig. S6B–S6D). No correlation was observed between the CD39 percentage and CD8 T cells in patients treated with FOLFIRINOX (**Fig. 5D**).

To further define which leukocyte subsets expressed CD39, lineage markers were used and showed $CD39^+CD45^+$ cells included primarily $CD14^+CD16^-$ classical monocytes (63.4%), $CD16^+CD14^-$ nonclassical monocytes (10.6%), $CD19^+$ B cells (10.2%), $CD4^+$ (7.6%), $CD16^-$ NK (3.4%) with $CD16^+$ NK, $CD8^+$ T cells, and NKT cells each less than 2% (**Fig. 5E** and **F**). These results show that while $CD39^+$ cells are heterogeneous, the majority of CD39-expressing cells are monocytes,

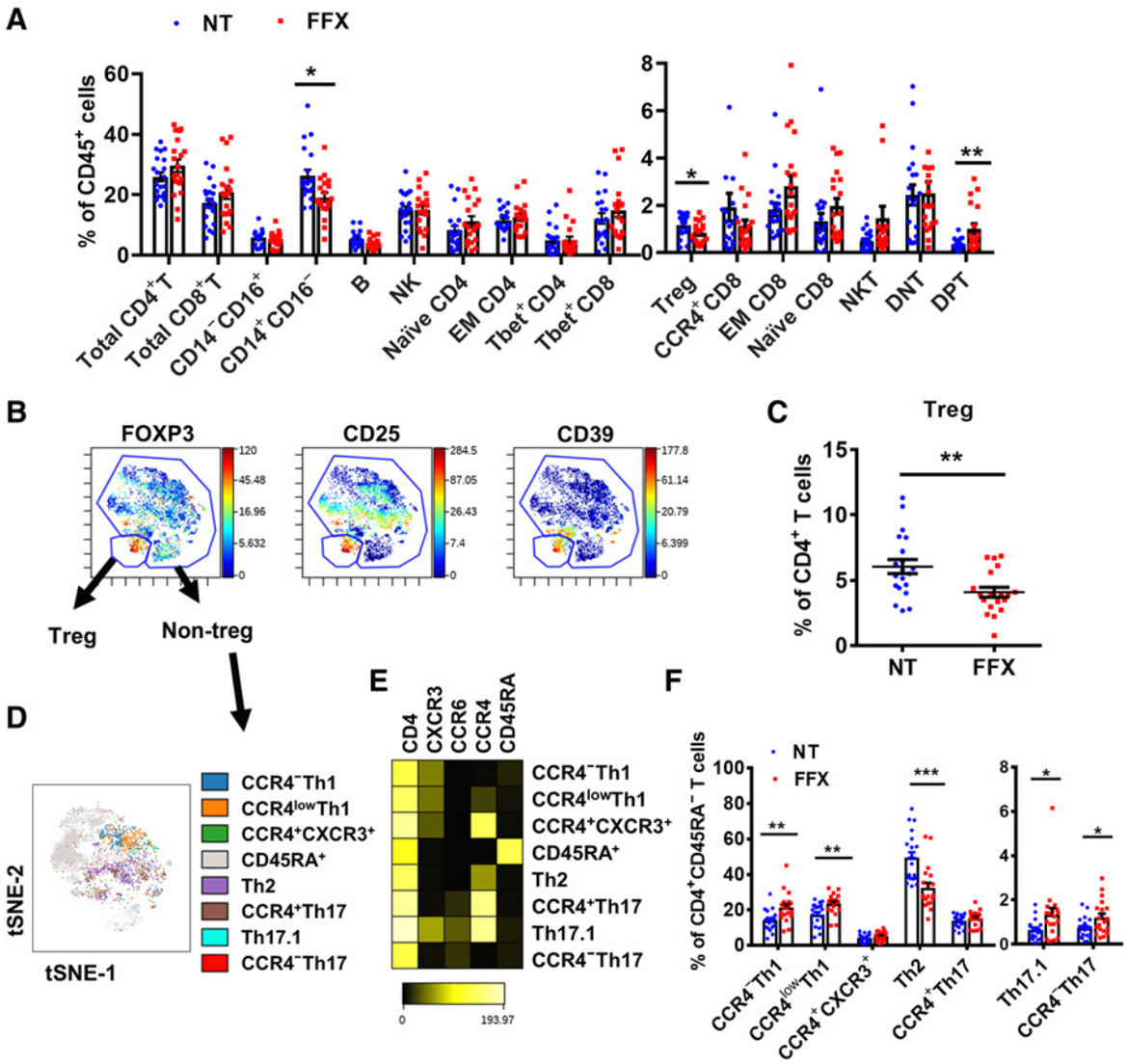

Figure 4.

FOLFIRINOX treatment is associated with decreased proportions of immune suppressor cells and increased proportions of effector cells. **A,** Percentage of total $CD4^+$ T cells ($CD4^+CD8^-CD3^+CD56^-$), total $CD8^+$ T cells ($CD4^-CD8^+CD3^+CD56^-$), NK cells ($CD56^+CD3^-$), NKT ($CD56^+CD3^+$), classical monocytes ($CD14^+CD16^-$), nonclassical monocytes ($CD14^-CD16^+$), DPT ($CD4^+CD8^+CD3^+CD56^-$), DNT ($CD4^-CD8^-CD3^+CD56^-$), B cells ($CD19^+CD3^-$), $Tbet^+CD4^+$ T cells, $Tbet^+CD8^+$ T cells, naïve $CD4^+$ T cells ($CD4^+CD45RA^+CCR7^+$), naïve $CD8^+$ T cells ($CD8^+CD45RA^+CCR7^+$), EM $CD4^+$T cells ($CD4^+CD45RA^-CCR7^-$), EM $CD8^+$ T cells ($CD8^+CD45RA^-CCR7^-$), $CCR4^+CD8^+$ T cells ($CCR4^+CD4^-CD8^+CD3^+CD56^-$), and Treg ($CD25^+FOXP3^+CD4^+CD3^+$) from treatment-naïve (NT, $n = 20$) and FOLFIRINOX-treated patients (FFX, $n = 19$). Graphical data represent the mean ± SEM and were analyzed by Mann–Whitney Wilcoxon test. *, $P < 0.05$ and **, $P < 0.01$. **B,** $CD4^+$ Treg ($CD39^+CD25^{hi}FOXP3^+$) and non-Treg subsets were identified by viSNE map after gating on $CD4^+CD3^+CD56^-$ cells. **C,** Percentage of $CD4^+$ Treg within total $CD4^+$ T cells in patients with PDAC. **D,** FlowSOM was used to generate the indicated $CD4^+$ T-cell subpopulations, and a heatmap summary of the expression values of lineage markers was used to distinguish cell subsets. **E,** The t-SNE algorithm was used to depict the immune populations in non-Treg CD4 T cells. **F,** The resulting cluster frequencies within $CD4^+CD45RA^-$T cells are shown in FOLFIRINOX-treated (FFX, $n = 19$) and treatment-naïve patients (NT, $n = 20$). Graphical data represent the mean ± SEM and were analyzed by Mann–Whitney Wilcoxon test. *, $P < 0.05$; **, $P < 0.01$; and ***, $P < 0.001$.

which could suppress T-cell function in the presence of ATP (37). This is further demonstrated by the lower levels of $CD8^+$ T cells found in patients with high CD39 levels.

Clinical responders to FOLFIRINOX are characterized by higher levels of effector T cells than nonresponders

Although FOLFIRINOX treatment decreased the proportion of suppressor cells, not all patients showed a clinical response to FOLFIRINOX, defined as greater than 30% tumor reduction. We subsequently examined differences in frequencies of the identified $CD45^+$ leukocyte clusters between clinical responders to FOLFIRINOX (FFX-R) and nonresponders (FFX-NR). The frequencies of CD8 T cells and $Tbet^+CD8^+$ T cells were significantly higher in responders than in nonresponders (**Fig. 6A**). Conversely, the frequency of $CD4^+$ Treg was significantly lower in FOLFIRINOX responders than in the nonresponder groups (**Fig. 6A**).

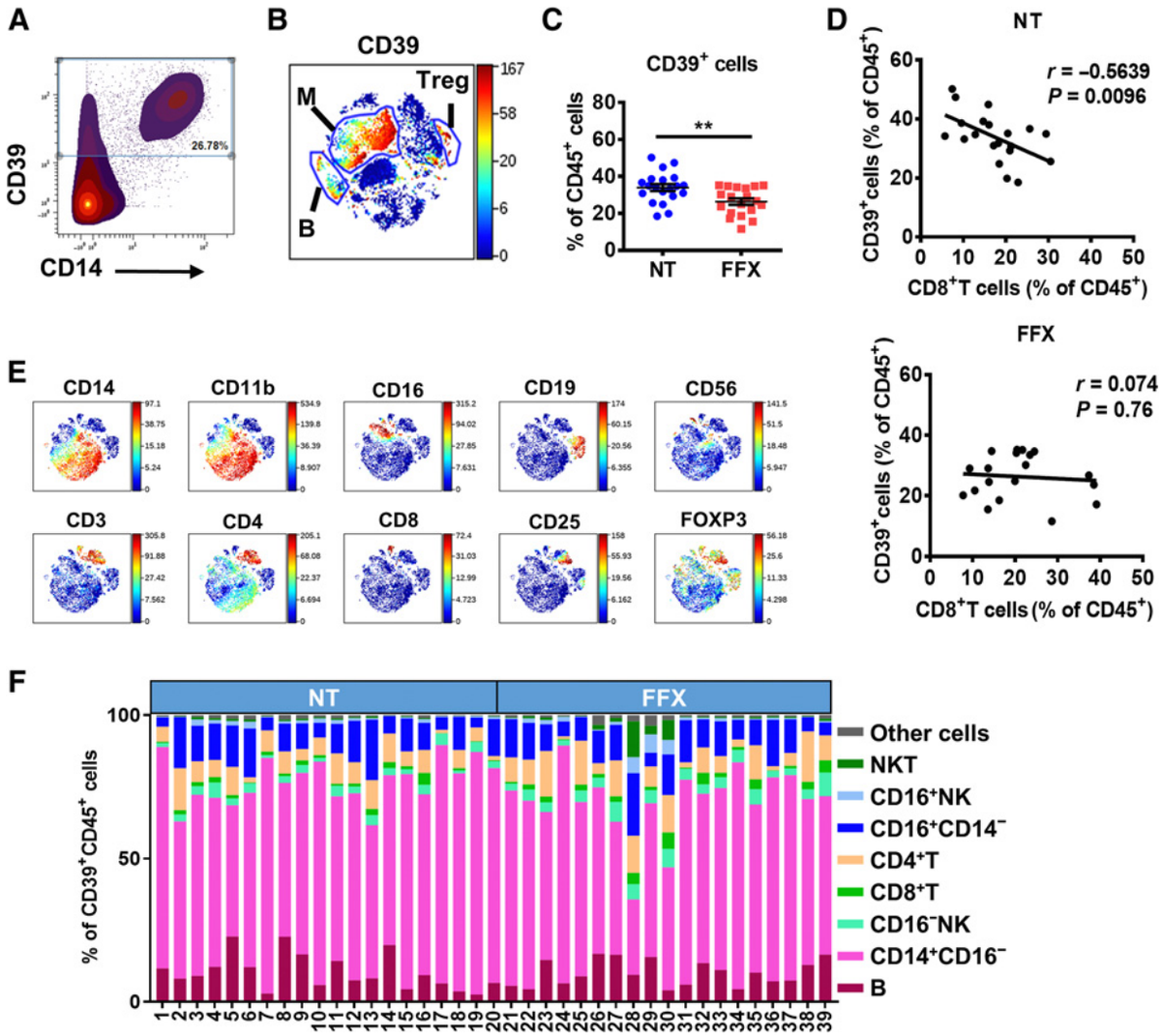

Figure 5.

CD39-expressing cells are reduced in FOLFIRINOX-treated patients compared with naïve treated patients. **A,** CD39 expression on $CD14^+$ cells. **B,** Two-dimensional cellular illustration of CD39 expression in PBMC by viSNE map (M = monocytes, B = B cells). **C,** Percentage of $CD39^+$ cells within total $CD45^+$ cells in FOLFIRINOX-treated patients (FFX, $n = 19$) and treatment-naïve patients (NT, $n = 20$). Graphical data represent the mean ± SEM and were analyzed by Mann–Whitney Wilcoxon test. **, $P < 0.01$. **D,** Correlation plots within a fitted linear regression line between frequency of $CD8^+$ T cells and the frequency of total $CD39^+CD45^+$ cells in untreated (NT, $N = 20$) and FOLFIRINOX-treated patients (FFX, $n = 19$). The P value was calculated using by Pearson correlation. **E,** Unsupervised clustering analysis with viSNE showing 2D cellular illustrations of CD3, CD4, CD8, CD14, CD16, CD11b, CD56, CD19, CD25, and FOXP3 within all $CD39^+$ cells. **F,** Distribution of cell subsets within $CD39^+CD45^+$ cells in individual patients.

To better characterize the phenotype of CD8 T cells, we gated on $CD3^+CD8^+CD56^-$ cells and performed a viSNE dimensional reduction (**Fig. 6B**). We found that $Tbet^+CD8^+$ T cells were divided into three distinct clusters: $CD27^-Tbet^+$, $CD27^+Tbet^+$, and $Ki67^+Tbet^+$ cells. Ki67 expression in CD8 T cells was reported previously as a marker of cellular proliferation and T-cell reinvigoration after checkpoint blockade therapy (38, 39). $Ki67^+Tbet^+$ $CD8^+$ T cells also express high levels of the cyclic ADP ribose hydrolase, CD38, which can increase cell proliferation (40). In our studies, the percentage of $Ki67^+Tbet^+CD8^+$ T cells trended higher in the responder group as compared with the nonresponder group; this difference was not statistically significant (**Fig. 6B**). We found the frequency of $CD27^-Tbet^+CD8^+$ T cells was significantly higher in responders compared with nonresponders (**Fig. 6B**). We further analyzed PD1 and GzmB expression in $CD27^-Tbet^+$ and $CD27^+Tbet^+$ subclusters and found that $CD27^-Tbet^+$ cells showed higher GzmB and lower PD1 than $CD27^+Tbet^+$ $CD8^+$ T cells (Supplementary Fig. S7), indicating $CD27^-Tbet^+CD8^+$ T cells might have higher effector function than $CD27^+Tbet^+$ $CD8^+$ T cells.

We also analyzed the expression of inhibitor receptors in CD8 T cells, including PD1, T-cell immunoreceptor with Ig and ITIM domains (TIGIT), T-cell immunoglobulin domain and mucin domain-3 (TIM-3), CTL antigen-4 (CTLA-4), and glucocorticoid-induced TNF family receptor (GITR). We observed that while some CD8 T cells expressed TIGIT and PD1, the proportions of $TIGIT^+CD8^+$T cells and $PD\text{-}1^+CD8^+$ T cells did not differ

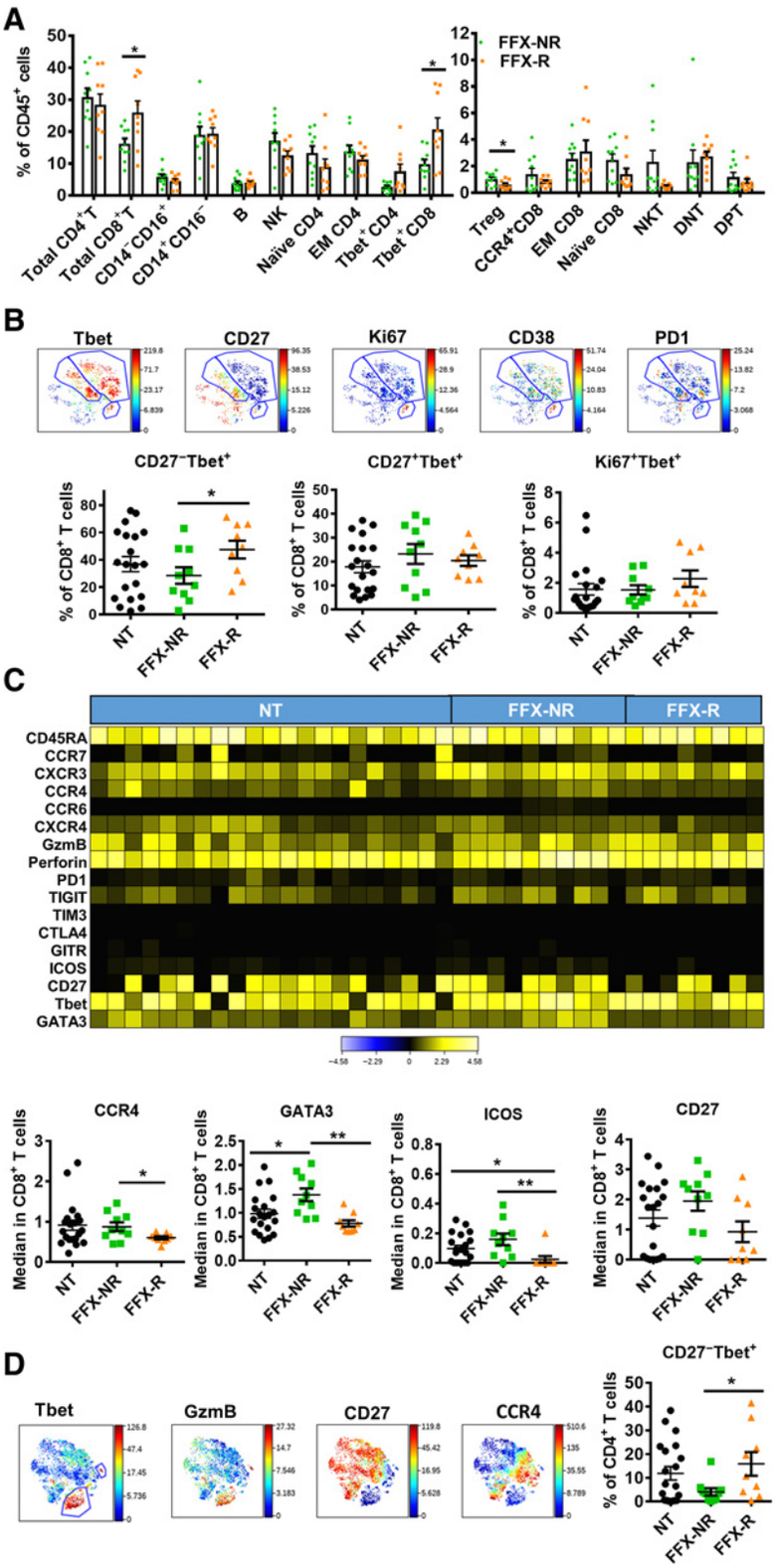

Figure 6.

Responders to FOLFIRINOX treatment are characterized by higher levels of effector T cells than non-responders. **A,** Percentage of total $CD4^+$ T cells, total $CD8^+$ T cells, NK cells, NKT, classical monocytes, nonclassical monocytes, DPT, DNT, B cells,$Tbet^+CD4^+$ T, $Tbet^+CD8^+$ T, naïve CD4 T cells, naïve CD8 T cells, EM CD4, EM CD8, $CCR4^+CD8$, and Treg in nonresponders to FOLFIRINOX (FFX-NR, $n = 10$) and responders to FOLFIRINOX (FFX-R, $n = 9$). Graphical data represent the mean ± SEM and were analyzed by Mann–Whitney Wilcoxon test. *, $P < 0.05$. **B,** $CD27^-Tbet^+$, $CD27^+Tbet^+$, and $Ki67^+Tbet^+$ subsets were identified with viSNE maps (top), and their prevalence is expressed as a percentage of total CD8 T cells in treatment-naïve (NT, $n = 20$), FFX-R ($n = 9$), and FFX-NR ($n = 10$) patients with PDAC (bottom). Graphical data represent the mean ± SEM and were analyzed by Mann–Whitney Wilcoxon test. *, $P < 0.05$. **C,** Heatmap of normalized median expression for markers expressed in CD8 T cells in treatment-naïve, FFX-NR, and FFX-R patients. Summary of normalized median expression for selected markers (CCR4, GATA3, ICOS, and CD27) in treatment-naïve (NT, $n = 20$), non-responders ($n = 10$), and responders to FOLFIRINOX treatment ($n = 9$). Graphical data represent the mean ± SEM and were analyzed by Mann–Whitney Wilcoxon test. *, $P < 0.05$ and **, $P < 0.01$. **D,** Left, $CD27^-Tbet^+$ subsets were identified within the CD4 T viSNE map. Right, Percentage of $CD27^-Tbet^+$ cells within total CD4 T cells in patients with PDAC with treatment-naïve (NT, $n = 20$), FFX-R ($n = 9$), and FFX-NR ($n = 10$). Graphical data represent the mean ± SEM, and data were analyzed by Mann–Whitney Wilcoxon test. *, $P < 0.05$.

between responders and nonresponders (**Fig. 6B** and **C**; Supplementary Fig. S8). On the other hand, GITR, CTLA4, and TIM3 were expressed in very few CD8 T cells in all groups (**Fig. 6C**; Supplementary Fig. S8). In addition, the median expression of GATA3, CCR4, and ICOS in total CD8 T cells was significantly higher in the nonresponder group than in the responder group (**Fig. 6C**). Because GATA3 has been demonstrated to drive the dysfunctional state in CD8 T cells (41), these results suggest increased presence of dysfunctional CD8 T cells in nonresponders compared with responders.

To better characterize the phenotype of CD4 T cells, we gated on $CD3^+CD4^+CD56^-$ cells and performed a viSNE analysis (**Fig. 6D**). The most notable, and significant difference between responders and nonresponders was observed in the $Tbet^{hi}CD4^+$ T cells that were confined to two individual cell clusters, and co-expressed high levels of GzmB but lacked CD27, CCR4, and CCR7, suggestive of effector/effector memory cells (**Fig. 6D**; Supplementary Fig. S9). Throughout **Fig. 6**, treatment-naïve patients are included for comparison with data that fall in between the responders and nonresponders to FOLFIRINOX.

Discussion

In this study, we analyzed the peripheral blood of patients with PDAC by CyTOF to characterize the immune cell signatures associated with FOLFIRINOX neoadjuvant therapy. After unsupervised clustering analysis of cell frequencies, we identified changes in CD4 T and monocytes in FOLFIRINOX-treated patients. Specifically, we observed reduced frequencies of suppressor cells, including classical monocytes and Treg in FOLFIRINOX-treated patients compared with treatment-naïve patients. Increased Th1 and decreased Th2 cell populations were also found in treated patients. Moreover, response to FOLFIRINOX was associated with an increased frequency of CD8 T cells, in particular $CD27^-Tbet^+$ effector/effector memory subsets. Overall, these data suggest that neoadjuvant chemotherapy with FOLFIRINOX may enhance effector T cells and downregulate suppressor cells, and CD8 T cells may play an important role in the response to FOLFIRINOX.

Our results are in line with other studies showing that some chemotherapeutics positively impact the immune system (9, 42). For example, treatment with oxaliplatin-cyclophosphamide controlled lung adenocarcinoma tumor progression in wild-type mice, but not in mice lacking CD8 T cells, suggesting the chemotherapy-induced antitumor response depends on host CD8 T cells (42). Here, we found that circulating CD8 T cells were significantly increased in FOLFIRINOX responders compared with nonresponders.

$CD27^-Tbet^+CD8^+$ T cells were upregulated in FOLFIRINOX responders compared with nonresponders and the median expression of GATA3, CCR4, and ICOS in CD8 T cells was significantly higher in FOLFIRINOX nonresponders than FOLFIRINOX responders. GATA3 has been reported as a regulator of CD8 T-cell dysfunction in melanoma (41) and T-bet is required for T-cell effector function during immunotherapy (43). Berrien-Elliott reported that dysfunctional T cells, characterized by low expression of T-bet and Eomes, have been rendered tolerant *in vivo* after encountering tumor antigens (43). Our results suggest the need for T-bet–expressing-CD8 effector T cells for the control of pancreatic cancer. Other than CD8 T cells, T-bet expression was observed in a variety of other immune subsets, including CD4 T cells and NKT cells, which could contribute to antitumor immunity. Consistent with this, we found a higher percentage of $CD27^-Tbet^+CD4^+$ T cells in responders compared with nonresponders. On the basis of CXCR3 and CCR6 expression, larger proportions of Th1 and Th17.1 cells were identified in PBMC from FOLFIRINOX-treated patients compared with treatment-naïve patients, suggesting FOLFIRINOX may also promote T-bet expression in CD4 T cells.

In a previous report, decreased levels of monocytes in the peripheral blood were associated with better survival in patients with pancreatic cancer (44). A follow-up study showed that blockade of tumor-induced recruitment of monocytes and granulocytes through small inhibitor molecules to CCR2 and CXCR2, respectively, augmented antitumor immunity and improved the response to FOLFIRINOX chemotherapy in murine pancreatic cancer models (45). Improved antitumor efficacy was dependent on CD8 T cells, as proven by loss of myeloid cell blockade efficacy in the absence of CD8 T cells (45). Here, we found $CD14^+CD16^-$ myeloid cells decreased in FOLFIRINOX-treated patients compared with treatment-naïve patients. Interestingly, the majority of the monocytes expressed CD39. CD39 is a surface-expressed immunomodulatory ecto-5′-nucleotidase that hydrolyzes extracellular ATP (36). ATP is a proinflammatory metabolite found in tumor interstitial fluid after chemotherapy-induced tumor cell death (31, 46). Thus, ATP may boost FOLFIRINOX-induced antitumor responses. In contrast, $CD39^+$ cells can suppress the functional activation of APC and T-cell responses (36). Our data are consistent with this notion, as CD8 T cells were negatively associated with $CD39^+$ cells in treatment-naïve patients with PDAC, and anti-CD39 mAb partially restored T-cell proliferation. The majority of $CD39^+$ cells in PBMC were $CD14^+$ cells, although B cells and $CD4^+$ Treg also expressed high levels of CD39. Thus, we speculate that in our earlier study (45), enhanced FOLFIRINOX chemotherapy-induced CD8 T-cell responses after blockade of myeloid cells might result from reduced numbers of $CD39^+$ cells. Of note, clinical targeting of the adenosine pathway, which involves CD39-mediated breakdown of ATP into AMP, is ongoing in patients with cancer (47).

A recent report showed that systemic immunity is essential for effective antitumor immune responses (46). Our results suggest that a response to FOLFIRINOX is associated with alterations in circulating immune subsets in patients with pancreatic cancer. As is well known, immunotherapy continues to emerge as an alternative treatment approach in patients with cancer. Unfortunately, immunotherapeutic approaches targeting T-cell immune checkpoints have not translated into clinical efficacy against PDAC due in part to a lack of activated T cells (21). Our study shows an increase in activated T cells in the blood of responders to FOLFIRINOX. This augmentation of T-cell responses after FOLFIRINOX neoadjuvant therapy provides the rationale for combinatory neoadjuvant therapy with FOLFIRINOX and blockade of the adenosine pathway (anti-CD39/anti-CD73/adenosine receptor blockade) or other forms of immunotherapy for patients with PDAC.

Several limitations of this study are noteworthy. First, the number of samples used in this study is limited and sampling of peripheral blood was performed at only one timepoint. It should be noted, however, that longitudinal sampling for analysis of immune status appears to reflect the impact of the tumor and/or treatment, and reportedly has predictive value (48, 49), suggesting that single timepoints are informative. Second, we note that the patients that underwent neoadjuvant therapy with FOLFIRINOX had more advanced disease at the time of diagnosis. However, not unexpectedly, the final pathologic stage was slightly lower in the neoadjuvant FOLFIRINOX group compared with the treatment-naïve group and is consistent with downstaging. The decision to do

chemotherapy first may be influenced by tumor location and factors like vascular abutment but drivers of cancer prognosis like size, nodal status, and distant spread are expected to be fairly homogeneous and almost certainly comparable from an immunologic perspective. Finally, we do not include immune profiling of PDAC tissue in this study. Mota Reyes and colleagues (22) concluded that neoadjuvant therapy depletes protumorigenic immune cells in PDAC tissue, as assessed through a combination of quantitative IHC and immune fluorescence. These findings in the tumor match our observations in peripheral blood. High-dimensional profiling of distinct areas within PDAC tumors by bulk proteogenomics, single-cell sequencing, and cellular imaging was recently performed at our institution (50), and we plan to use that data for a matched blood/PDAC tissue analysis.

In conclusion, chemotherapy that positively impacts an immune response may sensitize tumors to immune therapy and improve clinical outcomes in patients with PDAC.

Authors' Disclosures

D.R. Cullinan reports grants from NIH during the conduct of the study. J. Liu reports grants from NIH during the conduct of the study. W.E. Gillanders reports grants from NIH and Centene during the conduct of the study. W.G. Hawkins reports grants from NCI and Washington University-Centene ARCH Personalized Medicine Initiative during the conduct of the study as well as non-financial support from Celldex Corporation and other support from Accuronix Therapeutics outside the submitted work. No disclosures were reported by the other authors.

Authors' Contributions

H. Peng: Conceptualization, data curation, investigation, methodology, writing–original draft, writing–review and editing. **C.A. James:** Data curation, methodology. **D.R. Cullinan:** Data curation, methodology. **G.D. Hogg:** Data curation, methodology. **J.L. Mudd:** Resources, data curation. **C. Zuo:** Methodology. **R. Takchi:** Data curation. **K.E. Caldwell:** Writing-original draft, writing–review and editing. **J. Liu:** Data curation, methodology. **D.G. DeNardo:** Resources, writing–review and editing. **R.C. Fields:** Resources. **W.E. Gillanders:** Writing–review and editing. **S.P. Goedegebuure:** Conceptualization, supervision, writing–original draft, writing–review and editing. **W.G. Hawkins:** Conceptualization, resources, supervision, funding acquisition, writing–original draft, project administration, writing–review and editing.

Acknowledgments

This work was supported by NCI T32 CA009621 (C.A. James, K.E. Caldwell, D.R. Cullinan), The Washington University SPORE in Pancreas Cancer P50CA196510 (J.L. Mudd, G.D. Hogg, C. Zuo, J. Liu, D.G. DeNardo, R.C. Fields, W.E. Gillanders, S.P. Goedegebuure, W.G. Hawkins), and Centene Corporation contract P19-00559 (H. Peng, R. Takchi, S.P. Goedegebuure, D.G. DeNardo, R.C. Fields, W.E. Gillanders, W.G. Hawkins) for the Washington University-Centene ARCH Personalized Medicine Initiative.

The costs of publication of this article were defrayed in part by the payment of page charges. This article must therefore be hereby marked *advertisement* in accordance with 18 U.S.C. Section 1734 solely to indicate this fact.

Received March 20, 2021; revised June 21, 2021; accepted September 24, 2021; published first September 30, 2021.

References

1. Siegel RL, Miller KD, Jemal A. Cancer statistics, 2019. CA Cancer J Clin 2019;69:7–34.
2. Rahman SH, Urquhart R, Molinari M. Neoadjuvant therapy for resectable pancreatic cancer. World J Gastrointest Oncol 2017;9:457–65.
3. Hackert T. Surgery for pancreatic cancer after neoadjuvant treatment. Ann Gastroenterol Surg 2018;2:413–8.
4. Rangarajan K, Pucher PH, Armstrong T, Bateman A, Hamady Z. Systemic neoadjuvant chemotherapy in modern pancreatic cancer treatment: a systematic review and meta-analysis. Ann R Coll Surg Engl 2019;101:453–62.
5. Conroy T, Hammel P, Hebbar M, Ben Abdelghani M, Wei AC, Raoul JL, et al. FOLFIRINOX or gemcitabine as adjuvant therapy for pancreatic cancer. N Engl J Med 2018;379:2395–406.
6. Hackert T, Sachsenmaier M, Hinz U, Schneider L, Michalski CW, Springfeld C, et al. Locally advanced pancreatic cancer: neoadjuvant therapy with folfirinox results in resectability in 60% of the patients. Ann Surg 2016;264:457–63.
7. Costello E, Shibuya KC, Goel VK, Xiong W, Sham JG, Pollack SM, et al. Pancreatic ductal adenocarcinoma contains an effector and regulatory immune cell infiltrate that is altered by multimodal neoadjuvant treatment. PLoS One 2014;9:e96565.
8. Galluzzi L, Buqué A, Kepp O, Zitvogel L, Kroemer G. Immunological effects of conventional chemotherapy and targeted anticancer agents. Cancer Cell 2015;28:690–714.
9. Wang Y-J, Fletcher R, Yu J, Zhang L. Immunogenic effects of chemotherapy-induced tumor cell death. Genes Dis 2018;5:194–203.
10. Tel J, Hato SV, Torensma R, Buschow SI, Figdor CG, Lesterhuis WJ, et al. The chemotherapeutic drug oxaliplatin differentially affects blood DC function dependent on environmental cues. Cancer Immunol Immunother 2011;61:1101–11.
11. Ye J, Mills BN, Zhao T, Han BJ, Murphy JD, Patel AP, et al. Assessing the magnitude of immunogenic cell death following chemotherapy and irradiation reveals a new strategy to treat pancreatic cancer. Cancer Immunol Res 2020;8:94–107.
12. Feig C, Gopinathan A, Neesse A, Chan DS, Cook N, Tuveson DA. The pancreas cancer microenvironment. Clin Cancer Res 2012;18:4266–76.
13. Connor AA, Denroche RE, Jang GH, Timms L, Kalimuthu SN, Selander I, et al. Association of distinct mutational signatures with correlates of increased immune activity in pancreatic ductal adenocarcinoma. JAMA Oncol 2017;3:774–83.
14. Mitchem JB, Brennan DJ, Knolhoff BL, Belt BA, Zhu Y, Sanford DE, et al. Targeting tumor-infiltrating macrophages decreases tumor-initiating cells, relieves immunosuppression, and improves chemotherapeutic responses. Cancer Res 2012;73:1128–41.
15. Jang JE, Hajdu CH, Liot C, Miller G, Dustin ML, Bar-Sagi D. Crosstalk between regulatory T cells and tumor-associated dendritic cells negates anti-tumor immunity in pancreatic cancer. Cell Rep 2017;20:558–71.
16. Hegde S, Krisnawan VE, Herzog BH, Zuo C, Breden MA, Knolhoff BL, et al. Dendritic cell paucity leads to dysfunctional immune surveillance in pancreatic cancer. Cancer Cell 2020;37:289–307.
17. Liyanage UK, Moore TT, Joo HG, Tanaka Y, Herrmann V, Doherty G, et al. Prevalence of regulatory T cells is increased in peripheral blood and tumor microenvironment of patients with pancreas or breast adenocarcinoma. J Immunol 2002;169:2756–61.
18. De Monte L, Reni M, Tassi E, Clavenna D, Papa I, Recalde H, et al. Intratumor T helper type 2 cell infiltrate correlates with cancer-associated fibroblast thymic stromal lymphopoietin production and reduced survival in pancreatic cancer. J Exp Med 2011;208:469–78.
19. Ohlund D, Handly-Santana A, Biffi G, Elyada E, Almeida AS, Ponz-Sarvise M, et al. Distinct populations of inflammatory fibroblasts and myofibroblasts in pancreatic cancer. J Exp Med 2017;214:579–96.
20. Farren MR, Mace TA, Geyer S, Mikhail S, Wu C, Ciombor K, et al. Systemic immune activity predicts overall survival in treatment-naive patients with metastatic pancreatic cancer. Clin Cancer Res 2016;22:2565–74.
21. Balachandran VP, Beatty GL, Dougan SK. Broadening the impact of immunotherapy to pancreatic cancer: challenges and opportunities. Gastroenterology 2019;156:2056–72.
22. Mota Reyes C, Teller S, Muckenhuber A, Konukiewitz B, Safak O, Weichert W, et al. Neoadjuvant therapy remodels the pancreatic cancer microenvironment via depletion of protumorigenic immune cells. Clin Cancer Res 2020;26:220–31.
23. Therasse P, Arbuck SG, Eisenhauer EA, Wanders J, Kaplan RS, Rubinstein L, et al. New guidelines to evaluate the response to treatment in solid tumors. European Organization for Research and Treatment of Cancer, National Cancer Institute of the United States, National Cancer Institute of Canada. J Natl Cancer Inst 2000;92:205–16.

24. Finck R, Simonds EF, Jager A, Krishnaswamy S, Sachs K, Fantl W, et al. Normalization of mass cytometry data with bead standards. Cytometry A 2013;83:483–94.
25. Lun ATL, Richard AC, Marioni JC. Testing for differential abundance in mass cytometry data. Nat Methods 2017;14:707–9.
26. Hartmann FJ, Bernard-Valnet R, Queriault C, Mrdjen D, Weber LM, Galli E, et al. High-dimensional single-cell analysis reveals the immune signature of narcolepsy. J Exp Med 2016;213:2621–33.
27. Conroy T, Desseigne F, Ychou M, Bouche O, Guimbaud R, Becouarn Y, et al. FOLFIRINOX versus gemcitabine for metastatic pancreatic cancer. N Engl J Med 2011;364:1817–25.
28. Ferrone CR, Marchegiani G, Hong TS, Ryan DP, Deshpande V, McDonnell EI, et al. Radiological and surgical implications of neoadjuvant treatment with FOLFIRINOX for locally advanced and borderline resectable pancreatic cancer. Ann Surg 2015;261:12–7.
29. Macedo FI, Ryon E, Maithel SK, Lee RM, Kooby DA, Fields RC, et al. Survival outcomes associated with clinical and pathological response following neoadjuvant FOLFIRINOX or gemcitabine/nab-paclitaxel chemotherapy in resected pancreatic cancer. Ann Surg 2019;270:400–13.
30. Chawla A. Contemporary trials evaluating neoadjuvant therapy for resectable pancreatic cancer. J Surg Oncol 2021;123:1423–31.
31. Li X-Y, Moesta AK, Xiao C, Nakamura K, Casey M, Zhang H, et al. Targeting CD39 in cancer reveals an extracellular ATP- and inflammasome-driven tumor immunity. Cancer Discov 2019;9:1754–73.
32. Panni RZ, Herndon JM, Zuo C, Hegde S, Hogg GD, Knolhoff BL, et al. Agonism of CD11b reprograms innate immunity to sensitize pancreatic cancer to immunotherapies. Sci Transl Med 2019;11:eaau9240.
33. Song K, Rabin RL, Hill BJ, De Rosa SC, Perfetto SP, Zhang HH, et al. Characterization of subsets of CD4+ memory T cells reveals early branched pathways of T cell differentiation in humans. Proc Natl Acad Sci U S A 2005; 102:7916–21.
34. Hagihara K, Chan S, Zhang L, Oh DY, Wei XX, Simko J, et al. Neoadjuvant sipuleucel-T induces both Th1 activation and immune regulation in localized prostate cancer. Oncoimmunology 2018;8:e1486953.
35. Ramstein J, Broos CE, Simpson LJ, Ansel KM, Sun SA, Ho ME, et al. IFN-gamma-producing T-helper 17.1 cells are increased in sarcoidosis and are more prevalent than T-helper type 1 cells. Am J Respir Crit Care Med 2016;193:1281–91.
36. Moesta AK, Li X-Y, Smyth MJ. Targeting CD39 in cancer. Nat Rev Immunol 2020;20:739–55.
37. Perrot I, Michaud HA, Giraudon-Paoli M, Augier S, Docquier A, Gros L, et al. Blocking antibodies targeting the CD39/CD73 immunosuppressive pathway unleash immune responses in combination cancer therapies. Cell Rep 2019;27: 2411–25.
38. Huang AC, Postow MA, Orlowski RJ, Mick R, Bengsch B, Manne S, et al. T-cell invigoration to tumour burden ratio associated with anti-PD-1 response. Nature 2017;545:60–5.
39. Kamphorst AO, Pillai RN, Yang S, Nasti TH, Akondy RS, Wieland A, et al. Proliferation of PD-1+ CD8 T cells in peripheral blood after PD-1-targeted therapy in lung cancer patients. Proc Natl Acad Sci U S A 2017;114:4993–8.
40. Wei W, Graeff R, Yue J. Roles and mechanisms of the CD38/cyclic adenosine diphosphate ribose/Ca(2+) signaling pathway. World J Biol Chem 2014;5:58–67.
41. Singer M, Wang C, Cong L, Marjanovic ND, Kowalczyk MS, Zhang H, et al. A distinct gene module for dysfunction uncoupled from activation in tumor-infiltrating T cells. Cell 2016;166:1500–11.
42. Pfirschke C, Engblom C, Rickelt S, Cortez-Retamozo V, Garris C, Pucci F, et al. Immunogenic chemotherapy sensitizes tumors to checkpoint blockade therapy. Immunity 2016;44:343–54.
43. Berrien-Elliott MM, Yuan J, Swier LE, Jackson SR, Chen CL, Donlin MJ, et al. Checkpoint blockade immunotherapy relies on T-bet but not eomes to induce effector function in tumor-infiltrating CD8+ T cells. Cancer Immunol Res 2015; 3:116–24.
44. Sanford DE, Belt BA, Panni RZ, Mayer A, Deshpande AD, Carpenter D, et al. Inflammatory monocyte mobilization decreases patient survival in pancreatic cancer: a role for targeting the CCL2/CCR2 axis. Clin Cancer Res 2013; 19:3404–15.
45. Nywening TM, Belt BA, Cullinan DR, Panni RZ, Han BJ, Sanford DE, et al. Targeting both tumour-associated CXCR2(+) neutrophils and CCR2(+) macrophages disrupts myeloid recruitment and improves chemotherapeutic responses in pancreatic ductal adenocarcinoma. Gut 2018;67:1112–23.
46. Spitzer MH, Carmi Y, Reticker-Flynn NE, Kwek SS, Madhireddy D, Martins MM, et al. Systemic immunity is required for effective cancer immunotherapy. Cell 2017;168:487–502.
47. Leone RD, Emens LA. Targeting adenosine for cancer immunotherapy. J Immunother Cancer 2018;6:57.
48. Nywening TM, Wang-Gillam A, Sanford DE, Belt BA, Panni RZ, Cusworth BM, et al. Targeting tumour-associated macrophages with CCR2 inhibition in combination with FOLFIRINOX in patients with borderline resectable and locally advanced pancreatic cancer: a single-centre, open-label, dose-finding, non-randomised, phase 1b trial. Lancet Oncol 2016;17:651–62.
49. Toledano-Fonseca M, Cano MT, Inga E, Gomez-Espana A, Guil-Luna S, Garcia-Ortiz MV, et al. The combination of neutrophil-lymphocyte ratio and platelet-lymphocyte ratio with liquid biopsy biomarkers improves prognosis prediction in metastatic pancreatic cancer. Cancers 2021;13:1210.
50. Zhou DC, Jayasinghe RG, Herndon JM, Storrs E, Mo C-K, Wu Y, et al. Spatial drivers and pre-cancer populations collaborate with the microenvironment in untreated and chemo-resistant pancreatic cancer. bioRxiv 2021.